

Using the finite-difference time-domain pulse propagation method to simulate time-resolved THz experiments

Matthew C. Beard and Charles A. Schmuttenmaer^{a)}

Department of Chemistry, Yale University, 225 Prospect Street, New Haven, Connecticut 06520-8107

(Received 1 September 2000; accepted 14 November 2000)

The finite-difference time-domain (FDTD) method has been applied to time-resolved THz spectroscopy (TRTS) experiments. Time-resolved THz spectroscopy utilizes an optical pump pulse to excite the sample, followed by a far-infrared (FIR) probe pulse with frequency components that span from 10 to 100 cm^{-1} . The subpicosecond evolution of the FIR spectrum is obtained as a function of time after the visible photoexcitation event. Significant challenges arise in interpreting these experimental results due to the very different frequencies of the pump and probe pulses. Therefore, it is essential to simulate the experiment. The method described entails numerically propagating both the THz probe pulse and the visible pump pulse simultaneously, keeping track of the transiently induced polarization from absorption of the visible pulse. Group velocity mismatch between the visible and THz pulse and a transiently changing response function are completely accounted for in the calculation. Furthermore, a spatially varying polarization can be included to account for a nonuniform excited region of the sample under investigation. The response function of the material is described as a multimode Brownian oscillator that can describe dispersive media in a very general sense. In particular, the overdamped, underdamped, and critically damped cases are all included, as well as special cases such as a Debye or Drude response. As a specific example, we present results of modeling a TRTS experiment of photoexcitation of a dye in solution, namely, 2,11,20,29-tetra-*tert*-butyl-2,3-naphthalocyanine, dissolved in toluene. We carry out a nonlinear least squares fit of a parameterized model to the measured data to show that the FDTD-TRTS method is able to accurately reproduce the features observed in the measured data set. © 2001 American Institute of Physics. [DOI: 10.1063/1.1338526]

I. INTRODUCTION

Recent developments in time-resolved THz spectroscopy (TRTS) have enabled the measurement of the electric field of a nearly single-cycle THz pulse after it propagates through a photoexcited medium with subpicosecond temporal resolution.¹⁻⁶ This new visible pump, far-infrared (FIR) probe spectroscopy, has opened up the FIR region of the spectrum to time-resolved studies (which have proven to be of great utility in other regions of the spectrum). The FIR region contains important information relevant to chemistry, physics, and biology, and *time-resolved* studies in the FIR will provide new insights. Unique challenges exist to correctly collect and interpret data from TRTS experiments.^{4,6-8} These challenges arise because the THz probe pulses have large bandwidth in relation to their central frequency; hence, the slowly varying envelope approximation is not valid. In this article we discuss these challenges, and extend finite-difference time-domain (FDTD) pulse propagation methods to model TRTS experiments in order to extract time-dependent information.

FDTD methods are commonplace for solving complex problems for electromagnetic (EM) pulse propagation,^{9,10} but they have only recently been applied to EM propagation in dispersive media.¹¹⁻¹⁵ A dispersive medium is described by frequency-dependent material parameters: the absorption co-

efficient, $\alpha(\omega)$, and index of refraction, $n(\omega)$. Typically, Fourier transform (FT) methods are used to extract information from EM pulse propagation experiments, and these methods have been used successfully to interpret static THz spectra,^{16,17} unfortunately, they do not correctly describe a TRTS experiment. In this article, we show that FDTD calculations can reproduce the phenomena encountered in a TRTS experiment when the FT methods fail.

Three situations arise in TRTS experiments that hinder the use of FT methods.^{4,7,18} First, group velocity mismatch exists between the propagation of the visible and THz pulses in the dispersive medium. Second, the optical properties of the medium may change on the timescale of the THz pulse duration. Third, there might be a nonuniform spatial distribution of the photoexcited region in the material being studied. These situations are all correctly simulated in a FDTD calculation by numerically propagating both the visible and the THz pulses simultaneously. The transient polarization induced by propagation of the visible pulse influences the propagation of the THz pulse, and evolves according to the propagation of the visible pulse and the excited state properties. Thus, the THz pulse encounters a medium whose response is changing or has changed due to concurrent or prior propagation of the visible pulse. Herein lies the power of the FDTD method in simulating TRTS experiments: the optical properties of the medium are transiently modified *during* the

^{a)}Electronic mail: charles.schmuttenmaer@yale.edu

propagation of the THz pulse, which is exactly what occurs in the experiment.

This article is organized by first describing the static FDTD method for dispersive media. Then the multimode Brownian oscillator (MBO) time-domain response function is introduced and shown to be a general way to describe dispersive phenomena. These response functions are then incorporated into the FDTD method. Finally, the FDTD method is extended to include the visible pump pulse propagation to simulate TRTS experiments, and results of photo-excited 2,11,20,29-tetra-*tert*-butyl-2,3-naphthalocyanine (TBNC) in toluene are shown to illustrate the technique.

II. METHOD

A. Finite-difference time-domain propagation

A dispersive medium can be treated within the standard Yee FDTD method¹⁰ using several different methodologies. The three most common approaches are the recursive convolution (RC),^{11,12} the Z-transform method,¹⁴ and the auxiliary differential equation (ADE) method.¹⁵ While each method has its advantages and disadvantages,¹⁹ we have found the RC-FDTD method most useful for simulating TRTS experiments because it is most intuitive, easiest to implement, and general enough to simulate a wide variety of experiments. The only requirement of the RC-FDTD method is that the time-domain response function can be expressed in an exponential form, which is satisfied by the MBO response function. Lorentzian, Debye, and Drude responses are all specific cases of the MBO response function. Furthermore, the optical properties of an arbitrary medium can be expressed as a linear combination of simple MBO functions.

Because the beamwaists of the visible and THz beams are much larger than the penetration depth of the excitation pulse, we need consider only one dimension, but this method is easily generalizable to three dimensions. In one dimension, the Maxwell curl equations are

$$\begin{aligned}\nabla \times H &= \frac{\partial D}{\partial t} + J, \\ \nabla \times E &= -\frac{\partial B}{\partial t},\end{aligned}\quad (1)$$

where D is the displacement field, E is the electric field, B is the magnetic field, $H = \mu B$ (where μ is the permeability), and J is the current. For the following, J is replaced by the source current which is a reference THz pulse, and no other sources of current are included.

The RC-FDTD method is based on convolution of the material response function (or time-domain susceptibility), $\chi(t)$, with the electric field to obtain the electric displacement.^{11,12}

$$D(t) = \varepsilon_\infty \varepsilon_0 E(t) + \varepsilon_0 \int_0^t E(t-\tau) \chi(\tau) d\tau. \quad (2)$$

Discretization within the familiar Yee cell¹⁰ leads to the FDTD formula for Eq. (2) yielding^{11,12}

$$D^n(i) = \varepsilon_\infty \varepsilon_0 E^n(i) + \sum_{m=0}^{n-1} E^{n-m}(i) \int_{m\Delta t}^{(m+1)\Delta t} \chi(\tau) d\tau, \quad (3)$$

where $n\Delta t$ is the time, $i\Delta z$ is the distance, ε_∞ is the high frequency dielectric constant, and ε_0 is the permittivity of free space. If the material response function has an exponential form, then the summation in Eq. (3) can be recursively updated at each time step. Following Luebbers *et al.*,^{11,12} we define the following quantities:

$$\chi^m = \int_{m\Delta t}^{(m+1)\Delta t} \chi(\tau) d\tau, \quad (4)$$

$$\Delta \chi^m = \chi^m - \chi^{m+1}, \quad (5)$$

$$\psi^n = \sum_{m=0}^{n-1} E^{n-m} \Delta \chi^m. \quad (6)$$

The electric field update equation is then^{11,12}

$$\begin{aligned}E^{n+1}(i) &= \frac{\varepsilon_\infty}{\varepsilon_\infty + \chi^0} E^n(i) + \frac{1}{\varepsilon_\infty + \chi^0} \psi^n - \frac{\Delta t}{(\varepsilon_\infty + \chi^0) \varepsilon_0 \Delta z} \\ &\quad \times [H^{n+1/2}(i+1/2) - H^{n+1/2}(i-1/2)] - \frac{J_s(i) \Delta t}{\varepsilon_0},\end{aligned}\quad (7)$$

and magnetic field update is

$$\begin{aligned}H^{n+1/2}(i+1/2) &= H^{n-1/2}(i+1/2) \\ &\quad - \frac{\Delta t}{\mu \Delta z} [E^n(i+1) - E^n(i)].\end{aligned}\quad (8)$$

The source current J_s is given by

$$J_s(i) = \begin{cases} \frac{E_{\text{THz}}(t)}{Z}, & i=5 \\ 0, & i \neq 5 \end{cases}, \quad (9)$$

where $Z = \sqrt{\mu_0/\varepsilon_0}$ is the impedance of free space, and $E_{\text{THz}}(t)$ is the value of a reference THz pulse at time t . The reference pulse is generated at grid position No. 5, which is typically well in front of the sample cell position and five grid points in front of the boundary of the simulation space. Absorbing boundaries^{20,21} are used to absorb the backward going pulse as well as any reflections from the sample cell.

To propagate the pulse, we only need to obtain $\chi(t)$, as described below, and then evaluate Eqs. (7) and (8).

B. MBO response function

The MBO response function is described by a solution of the generalized Langenvin equation (GLE) of motion.²² If we average over thermal fluctuations and make the Markovian approximation (constant damping coefficient, γ), then the GLE reduces to

$$\ddot{s}_j(t) + \omega_j^2 s_j(t) + 2\gamma_j \dot{s}_j(t) = \sqrt{\frac{\eta_j \varepsilon_0}{m_j^* V}} E(t), \quad (10)$$

where, s_j is the macroscopic mode coordinate that represents the expectation value over all microscopic orientations and phases of the j th mode, ω_j is the j th oscillator frequency, γ_j is the j th damping coefficient, η_j is the coupling of the j th mode to the driving field $E(t)$, m^* is the effective mass of the oscillator, and V is the volume. This is simply the equation of motion for a damped, driven harmonic oscillator with force constant $k_j = \omega_j^2$ and damping coefficient $\delta_j = 2\gamma_j$.

The response function of a medium determines the contribution to the polarization at time t from an electric field at prior times; this contribution is

$$P(t) = \epsilon_0 \int_0^t E(t, \tau) \chi(\tau) d\tau. \quad (11)$$

This is the second term of Eq. (2). $\chi(\tau)$ can be obtained by considering the delta function impulse response to the equation of motion^{7,23} [Eq. (10)] and is given by²⁴

$$\chi_j(t) = \theta(t) \exp(-\gamma_j t) [A_1 \exp(\beta_j t) + A_2 \exp(-\beta_j t)], \quad (12)$$

where $\beta_j = \sqrt{\gamma_j^2 - \omega_j^2}$ and β may be either real ($\omega_j < \gamma_j$) or imaginary ($\omega_j > \gamma_j$), and $\theta(t)$ is the Heaviside step function at $t=0$. If $A_1 = -A_2 = \eta_j / (2\beta_j)$ then we recover the Lorentzian response, and when $\omega_j = 0$ also holds, we recover the Drude response. If $A_1 = 0, A_2 = \eta_j / (2\beta_j)$, then we recover the Debye response when $\omega_j = 0$.

For example, the time-domain Lorentzian response is given by

$$\chi_j(t) = \frac{\eta_j}{2\beta_j} \exp(-\gamma_j t) [\exp(\beta_j t) - \exp(-\beta_j t)], \quad (13)$$

and the frequency-domain response is given by the Laplace transform of Eq. (13):

$$\chi_j(\omega) = \frac{\omega_j^2 G_j (\epsilon_s - \epsilon_0)}{\omega_j^2 + 2i\omega\gamma_j - \omega^2}, \quad \chi_j(\nu) = \frac{\nu_j^2 G_j (\epsilon_s - \epsilon_\infty)}{\nu_j^2 + 2i\nu\gamma_j' - \nu^2}, \quad (14)$$

where $\omega = 2\pi\nu$, $\gamma_j = 2\pi\gamma_j'$ and $\eta_j = \omega_j^2 G_j (\epsilon_s - \epsilon_\infty)$, ϵ_s is the static dielectric constant and $G_j = (\epsilon_{j-1} - \epsilon_j) / (\epsilon_s - \epsilon_\infty)$, where ϵ_j describes the j th intermediate value of the dielectric constant.

Equation (12) is valid for underdamped or overdamped oscillators, as long as β is allowed to be complex. There are three distinct cases of damping:

underdamped: $\omega_j > \gamma_j$, $\beta_j = i\sqrt{\omega_j^2 - \gamma_j^2}$;

critically damped: $\omega_j = \gamma_j$, $\beta_j = 0$;

overdamped: $\omega_j < \gamma_j$, $\beta_j = \sqrt{\gamma_j^2 - \omega_j^2}$.

Equation (12) approaches the critically damped case smoothly from either side, but is incorrect for the exact case of critically damping. We treat cases of critical damping by increasing ω_i by one part in 10^5 . Figure 1 shows plots of the response function for the three cases, and the special cases of Drude and Debye overdamping when $\omega_j = k_j = 0$. Previous workers have used the RC-FDTD method for underdamped,¹² Debye,¹⁹ and Drude¹¹ oscillators, but it has never been applied to the general overdamped case with k_j

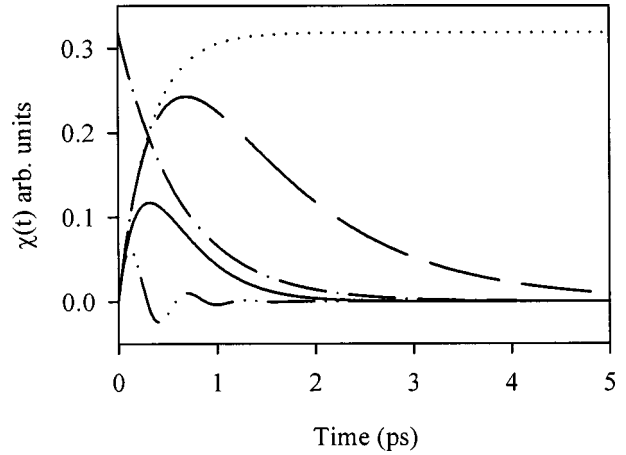


FIG. 1. Plots of the time-domain response function for several different cases of the MBO. The solid line is critically damped behavior, and the long dashed line is for overdamped. The dash-dot-dotted line is for underdamped, the dotted line is for the Drude response, and the dash-dotted line is the Debye response. With the RC-FDTD method described in the text we are able to model any combination of these dielectric responses.

$\neq 0$. We show here that the RC-FDTD method can be applied to a general Brownian oscillator; both underdamped and overdamped motions can be modeled with complete generality. This is essential for FIR studies since the majority of response functions encountered are overdamped. The approach for the underdamped case cannot be implemented for the general overdamped case simply by allowing β to be real. Our general approach outlined below is based on their approach for the underdamped case.¹²

To implement the RC-FDTD method we evaluate the integral in Eq. (4), determine the convolution term of Eq. (6), and evaluate Eqs. (7) and (8). For convenience, we split the response function in Eq. (12) into two parts, χ_1 and χ_2 , and evaluate each individually. For the Lorentzian response of Eq. 13 we obtain

$$\chi_{1,j}^m = \frac{A_{1,j}}{(\beta_j - \gamma_j)} \exp[m\Delta t(-\gamma_j + \beta_j)] \times \{\exp[\Delta t(-\gamma_j + \beta_j)] - 1\}, \quad (15)$$

$$\chi_{2,j}^m = \frac{-A_{2,j}}{(\beta_j + \gamma_j)} \exp[m\Delta t(-\gamma_j - \beta_j)] \times \{\exp[\Delta t(-\gamma_j - \beta_j)] - 1\}. \quad (16)$$

The response function χ at time step $m+1$ is related to the previous value by

$$\chi_j^{m+1} = \chi_{1,j}^m \exp[\Delta t(-\gamma_j + \beta_j)] + \chi_{2,j}^m \exp[\Delta t(-\gamma_j - \beta_j)], \quad (17)$$

and, therefore,

$$\Delta \chi_{1,j}^m = \chi_{1,j}^m \{1 - \exp[\Delta t(-\gamma + \beta)]\}, \quad (18)$$

$$\Delta \chi_{2,j}^m = \chi_{2,j}^m \{1 - \exp[\Delta t(-\gamma - \beta)]\}.$$

The convolution term in Eq. (6) can be updated as follows:

$$\psi_{1,j}^n(i) = E(i) \Delta \chi_{1,j}^0 + \exp[\Delta t(-\gamma_j + \beta_j)] \psi_{1,j}^{n-1}, \quad (19)$$

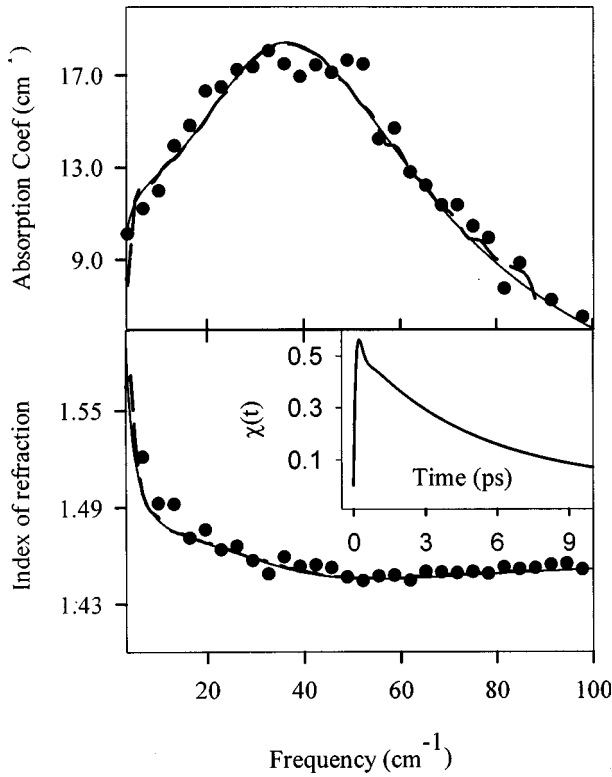


FIG. 2. Static FIR absorption and refractive index of chloroform along with the best fit in the frequency domain and FDTD propagation. The points are the measured data, the solid line is the best fit line, and the dashed line (virtually indistinguishable from the solid line) is the FDTD result. The best fit values were $\bar{\nu}_1=41.604 \text{ cm}^{-1}$, $\bar{\gamma}_1=30.56 \text{ cm}^{-1}$, $\bar{\nu}_2=6.57 \text{ cm}^{-1}$, $\bar{\gamma}_2=20.40 \text{ cm}^{-1}$, $\epsilon_s=4.801$, $\epsilon_1=4.702$, and $\epsilon_\infty=2.13$. The inset is the time-domain response function.

$$\psi_{2,j}^n(i) = E(i) \Delta \chi_{2,j}^0 + \exp[\Delta t(-\gamma_j - \beta_j)] \psi_{2,j}^{n-1}, \quad (20)$$

$$\psi_j^n = \psi_{1,j}^n + \psi_{2,j}^n, \quad (21)$$

with the initial time step $\psi_j^0=0$. Thus, for each oscillator j we need two additional real update terms if β is real and two complex update terms if β is complex, $\psi_{1,j}$, and $\psi_{2,j}$. To obtain the quantities needed in the E field update of Eq. (7), we sum over all the oscillators (poles) which describe the material parameters, taking the real part if β is complex, $\psi^n = \sum_j \text{Re}[\psi_j^n]$, and $\chi^m = \sum_j \text{Re}[\chi_j^m]$. Note that for the underdamped case, β_j in Eqs. (13), (15), and (16) is complex and thus so are ψ_j and χ_j . Before using these quantities in Eqs. (7) and (8) the real part is taken as described above.

We can also apply this approach to a system with two or more independent response functions, such as a homogeneous mixture²⁵ where $\epsilon = \sum_i f_i \epsilon_i$, where ϵ is the overall complex dielectric function, and ϵ_i the dielectric functions of the individual components with volume fraction f_i . We find that for each additional component of the mixture, two additional update terms per oscillator are required.

III. RESULTS

A. Static FDTD results

As an example of applying the above FDTD formalism to an overdamped oscillator, we present the results of simu-

lating the transmission of a THz pulse through neat CHCl_3 . The static FIR spectrum of CHCl_3 is shown in Fig. 2. The data were obtained by measuring the THz transmission through a variety of path lengths and extracting the absorption and index of refraction from a Beer's law analysis as described in Ref. 26. A double (two-pole) MBO model was fitted to the data in the frequency domain with the resulting parameters given in the Fig. 2 caption. The inset of Fig. 2 displays the time-domain response function. One oscillator is overdamped and one is underdamped. This static experiment was then simulated with the extended RC-FDTD method, the results are compared to the experiment, and the MBO fit in the frequency domain. This verifies that the FDTD method can reproduce the static experiment for both underdamped and overdamped oscillators. Furthermore, we have verified that the FDTD method can reproduce any combination of MBO responses: Drude, Debye, underdamped, overdamped, and critically damped. It is essential that in the static limit all of the cases be dealt with accurately before proceeding to the time-resolved situation, because the oscillators may change from one limit to another. For example, an oscillator may change from underdamped to overdamped upon photoexcitation.

B. TRTS-FDTD method

Extension of the FDTD method to time-resolved simulations is achieved by including the effects of the visible photoexcitation on the THz pulse propagation. In principle, a separate FDTD treatment of the visible pump pulse could be performed. This is not necessary, however, since it experiences very little dispersion because the absorption coefficient and index of refraction of the medium are essentially constant over the bandwidth of the pulse. The visible pulse propagates according to its group velocity in the material, and is attenuated according to Beer's law. The primary effect of the visible pulse is that it changes the material parameters governing propagation of the THz pulse. These effects are included by providing spatial and temporal dependencies to the response function, i.e., $\chi_j(t) \rightarrow \chi_j(t, t'', z)$, where t'' represents the relative delay between the visible and THz pulses prior to entering the sample, and z is the distance into the sample the pulses have propagated. With these two additions, a wide variety of TRTS experiments can be simulated.

For example, consider Fig. 3, which displays a THz pulse as it propagates from left to right through a hypothetical photoexcited medium at three different pump-probe delay times. The vertical line represents the interface of air and the material under investigation. The solid and dashed traces represent the THz pulse and the transient polarization induced by the visible pulse, respectively. The FIR optical properties are altered by absorption of the visible pump pulse, which is taken to have a Gaussian temporal profile. The properties return to their nonphotoexcited values with an exponential lifetime. Therefore, the temporal dependence of the transient polarization is a convolution of a Gaussian and an exponential function. The propagation time of the THz pulse is the same in each of the three panels, and only the relative delay of the pump pulse has been changed. In Fig.

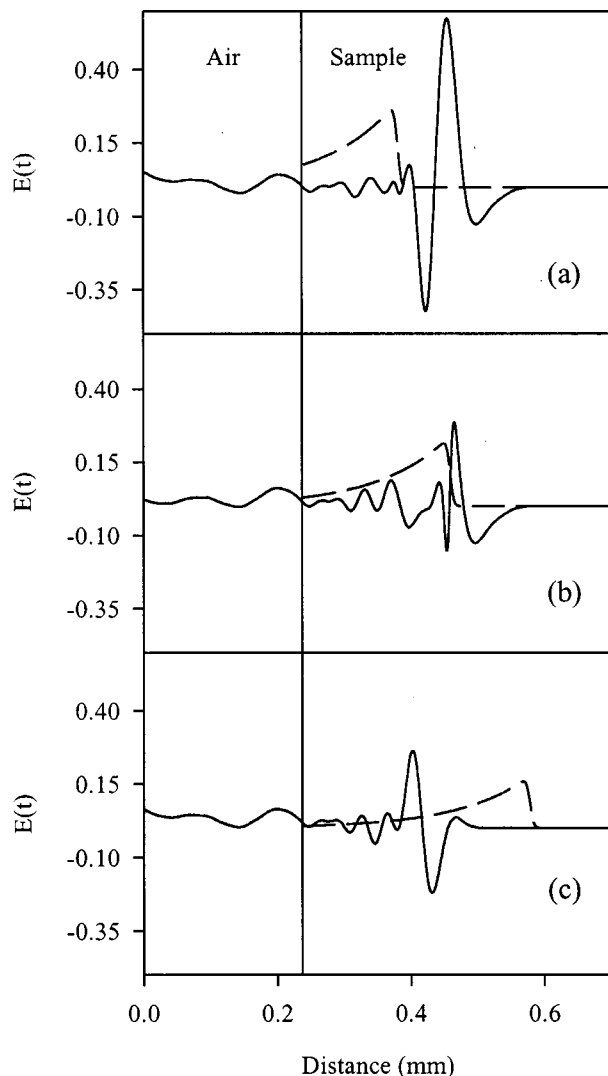


FIG. 3. TRTS-FDTD simulation. The THz pulse has propagated the same amount of time in each panel. The solid line is the THz pulse and the dashed line represents the transient polarization resulting from the propagation of the visible pulse. In (a) the pump pulse comes before the THz pulse, in (b) the pump pulse arrives at the same time as the THz pulse, and in (c) are effects of the pump pulse arriving before the THz pulse.

3(a) the pump pulse arrives after the main part of the THz pulse, however, the trailing edge of the THz pulse is still affected by it. In Fig. 3(b) the pump pulse arrives in the middle of the THz pulse, and the THz pulse is strongly distorted by the changing optical constants. Finally, in Fig. 3(c) the pump pulse arrives well before the THz pulse. However, the THz pulse still experiences different material parameters for different parts of the pulse due to the short lifetime of the excited state parameters chosen. The pump pulse intensity is seen to decrease from Fig. 3(a) to Fig. 3(c) due to the absorption of the visible pulse as it propagates through the medium.

To avoid numeric errors we have found that the time and distance grid steps must be at least 10–100 times smaller than any variations in either the temporal¹³ or spatial scale of the simulation. In addition, the Courant stability criterion²⁷ that $\Delta z/\Delta t \geq c/n_{\text{THz}}$ must be adhered to, where n_{THz} is the index of refraction for the THz pulse. In our simulations, the

pump pulse width is about 100 fs, which limits the time step to 10 fs and consequentially the distance step to 3 μm . If the absorption depth is smaller than 30 μm , however, then the spatial scale will be the limiting factor. We typically perform simulations at 0.8 times the Courant stability criterion.

C. TBNC/toluene simulations

As a specific example of the TRTS-FDTD method we present results of simulating a TRTS experiment. A dye molecule, TBNC, is dissolved in toluene and photoexcited by the visible pulse, after which the solvent molecules are probed by the THz pulse. The goal of this experiment is to probe the low frequency collective modes of the solvent in response to the perturbation by the excited solute. The visible pulse excites TBNC into its lowest excited electronic state, which has a different charge distribution than its ground state, and the solvent molecules respond to this new charge distribution. Roughly 5% of the solvent molecules, those participating in the solvation process, are affected by this perturbation.

Instantaneous electronic responses can contribute to the signal in addition to the nuclear response. We attribute the response close to time $t=0$, when the two pulses are overlapped, to electronic processes, while those that persist for longer times are attributed to a nuclear or molecular contribution. Therefore, we add an electronic response to our model which is active only during the duration of the pump pulse. In summary, we treat the photoexcited sample as a mixture of three types of oscillators whose populations are time dependent: nonphotoexcited oscillators, photoexcited oscillators, and an oscillator that corresponds to an instantaneous electronic response.

The response function is given by

$$\chi(t, t'', z) = f_e(t, t'', z)\chi_e(t) + [1 - f_e(t, t'', z)]\chi_0(t) + a(t, t'', z)\chi_{\text{elec}}(t), \quad (22)$$

where $f_e(t, t'', z)$ is the “population” of excited oscillators at time $t-t''$ and position z . The fraction not affected by photoexcitation is simply $1 - f_e(t, t'', z)$. The contribution of the instantaneous response is given by $a(t, t, z)$. The excited, nonexcited, and electronic response functions are $\chi_e(t)$, $\chi_0(t)$, and $\chi_{\text{elec}}(t)$, respectively.

The temporal dependence of the excited nuclear oscillators is given by the convolution of the visible pulse (taken as a Gaussian function) and a single exponential decay that has an optional long time offset. The spatial dependence is a single exponential function determined from the absorption coefficient of the dye solution. Thus, the excited “population” is given by

$$\begin{aligned} f_e(t, t'', z) &= g(t'', t) \otimes (e^{-t''/\tau} + b) \exp(-\alpha z) \\ &= f_0 \exp(-\alpha z) \int_{-\infty}^{\infty} \exp\left[-\left(\frac{t' - t''}{\Delta w}\right)^2\right] \\ &\quad \times \left[\exp\left(\frac{t'}{\tau}\right) + b \right] dt', \end{aligned} \quad (23)$$

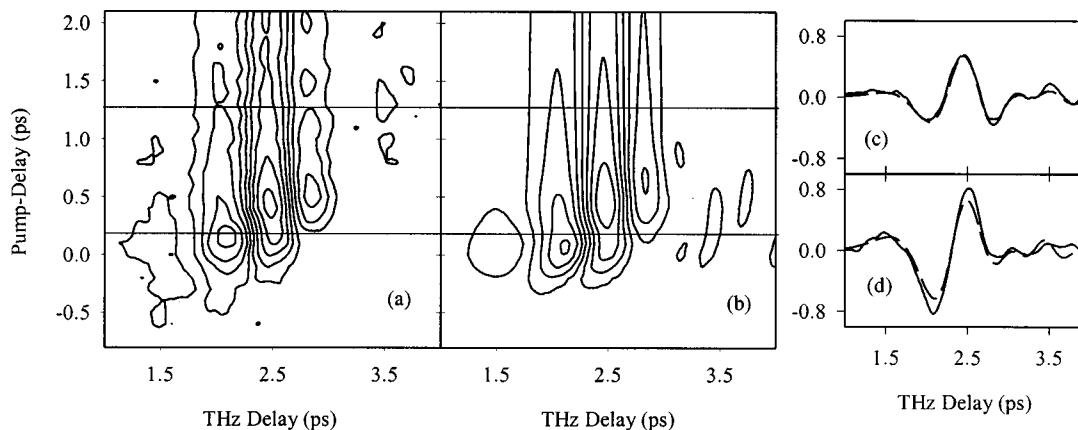


FIG. 4. Two-dimensional contour plot of the THz difference scan (pump on–pump off). (a) Experimental data and (b) FDTD–TRTS results found by the best nonlinear least squares fit to the data employing the model described in the text and parameters given in Table I. (c) Cuts taken at 1.3 ps (as indicated by the upper line on the two grids). The measured data are shown by the solid line, and the calculated data are shown by the dashed line. (d) Identical to (c), except that the cut is taken at 0.2 ps.

where $g(t'', t)$ is a Gaussian function representing the visible pulse, \otimes denotes a convolution, τ is the lifetime of the excited oscillators, b is the long time offset, α is the absorption coefficient of the dye solution, Δw is the full width at half maximum of the Gaussian pump pulse, f_0 is a scaling parameter that normalizes the convolution of the Gaussian function with the exponential, then scales it by $f_{e, \max}$ which approximately represents the volume fraction of solvent molecules which are affected by one laser pulse, $t' = t - (zn_{\text{vis}}/c)$ is the effective propagation time into the sample where n_{vis} is the index of refraction for the visible pulse, and c is the speed of light.

The time dependence of the electronic contribution is given by $a(t, t', z)$, which is taken to be the same Gaussian function that represents the visible pulse described in Eq. (23) and multiplied by the same spatial dependency $\exp(-\alpha z)$. For convenience, the electronic response function χ_{elec} is taken to be a Lorentzian function whose coupling to the field is given by the product $\Delta \epsilon_{\text{elec}} \nu_{\text{elec}}^2$.

Discretization of Eq. (23) is accomplished by numerically calculating the convolution term at the start of the simulation for each point in the simulation space and saving the results. Depending on the time step size and the length of the simulation, this can become quite a large calculation. Therefore, we typically calculate the convolution every 10 steps and interpolate to obtain a value at each point in the simulation space. Then, during the simulation we simply “look up” the appropriate value of $f_e(t, t'')$ and multiply by $\exp[-(i-i_0)\Delta z\alpha]\theta(i-i_0)$, where i_0 is the position of the sample in the simulation space and $\theta(i-i_0)$ is the Heaviside step function.

This is achieved by calculating the following convolution at the start of the simulation:

$$F(t_d) = g(t_d) \otimes \left[\exp\left(\frac{t_d}{\tau}\right) + b \right], \quad (24)$$

where $F(t_d)$ represents the population at the dummy time variable t_d . At each time step n during the simulation we

find the value of $F(t_d)$ which corresponds to $t_d = n\Delta t - (i\Delta zn_{\text{vis}}/c) + t''$. The convolution needs to be calculated only once for the entire simulation.

The model also includes effects of the quartz cuvette. We propagate the THz pulse through the cuvette, both before and after the sample in order to account for slight dispersion and absorption. The reference THz pulse used is the measured reference pulse which has been propagated backwards in time through the nonphotoexcited toluene solution and quartz cuvette. In addition, we account for propagation and distortion through the detector.¹⁸

We employ a nonlinear least squares fitting routine to adjust the parameters in our model to obtain the best fit. The nonexcited parameters of toluene are fit well by a single overdamped MBO oscillator and are held fixed during the fit. Ten parameters were allowed to vary during the fit, which brings up the issue of becoming trapped in a local minimum. There are three reasons that we feel the parameters are determined, unambiguously however. First, the correlations among parameters were quite low. For example, the highest correlation was between $\Delta \epsilon_{\text{elec}}$ and ν_{elec} , and was only 0.73. Second, these are the results of a global fit. That is, these parameters simultaneously describe 30 individual scans, each of which is 512 points long, for a total of 15 360 data points included in the fit. Third, the feature at a THz delay of ~ 2.9 ps that grows in later than the two primary features at 2.1 and 2.5 ps is very sensitive to the values of the parameters, particularly the instantaneous electronic contribution.

The results of the FDTD–TRTS fit are shown in Fig. 4 and it is seen that the agreement is quite good. Figure 4(a) displays a contour plot of the measured data and Fig. 4(b) is the best fit calculated data with the parameters given in Table I. Figures 4(c) and 4(d) are representative cuts at pump–probe delay times of 1.3 and 0.2 ps, respectively, which compare the calculated and measured data. We collect the data as described in Refs. 7 and 18 such that every portion of the probe has experienced the same delay from the pump beam. This is achieved numerically by calculating the data as described above and then projecting it onto constant values

TABLE I. Parameters from the results of the nonlinear least squares best fit to the measured data. One sigma uncertainties are given in parentheses. The conversion between cm^{-1} and frequency is $\nu=c\bar{\nu}$, $\gamma=c\bar{\gamma}$, where c is the speed of light.

| Parameter | Nonexcited oscillators | Excited oscillators |
|-------------------------------|------------------------------|-----------------------------|
| $\Delta\epsilon$ (electronic) | ... | 0.28 (0.01) |
| $\bar{\nu}$ (electronic) | ... | 26.1 (0.4) cm^{-1} |
| $\bar{\gamma}$ (electronic) | ... | 54 (1) cm^{-1} |
| ϵ_s (nuclear) | 2.19 (fixed) | 2.83 (0.02) |
| ϵ_∞ (nuclear) | 2.15(fixed) | 2.15 (fixed) |
| $\bar{\nu}$ (nuclear) | 159 cm^{-1} (fixed) | 156 (1) cm^{-1} |
| $\bar{\gamma}$ (nuclear) | 297 cm^{-1} (fixed) | 89.9 (0.5) cm^{-1} |
| τ | 0.47 (0.01) ps | |
| b | 0.49 (0.01) ps | |
| Δw | 150 fs (fixed) | |
| α | 400 cm^{-1} (fixed) | |
| $f_{e,\text{max}}$ | 0.05 (fixed) | |

of $t-t''$. It is seen from Table I that the Lorentzian oscillator representing the solvent changes from overdamped to underdamped upon photoexcitation of the dye molecule and that the static dielectric constant increases slightly. Both of these results are consistent with a ‘‘stiffening’’ of the liquid that surrounds the dye molecule. The decay time τ corresponds to the solvation time of the excited dye molecules. A more complete discussion of the underlying physics of these results will follow in a separate paper in which we compare these results with other TBNC/solvent systems.

IV. CONCLUSIONS

The RC-FDTD propagation method has been extended in two ways. First, it is now possible to treat any type of MBO response: underdamped, overdamped, critically damped, Drude model, or Debye model. Second, and more important, the RC-FDTD method can now treat situations where the material response parameters are changing temporally and spatially. These developments are necessary to properly simulate THz pulse propagation through photoexcited media, and thereby understand results of TRTS experiments.

The generality of our extended FDTD method allows arbitrary spatial distributions of photoexcited species to be considered. That is, we need not limit them to a slab, or an exponentially decreasing distribution. Any ‘‘back surface’’ reflections at the interface between the photoexcited and nonphotoexcited regions of the sample are automatically included, even if there is not a sharp boundary separating the two regions. For arbitrary spatial distributions we replace the $\exp(-\alpha z)$ term in Eq. (23) with appropriate spatial distribution.

With the scheme outlined above it is possible to include a wide variety of dynamics other than that described by Eq. (22). In fact, we have applied this technique to photoexcited electrons in GaAs.⁴ For those results we must include a time-

dependent scattering rate as the electrons relax to the bottom of the conduction band after being initially photoexcited. Furthermore we can model situations where a THz pulse is generated by a sample that is excited by a visible pulse as both propagate through a material which is dispersive.²⁸ Simulating TRTS experiments with the FDTD method is essential for correctly interpreting the temporal evolution of the FIR spectrum.

ACKNOWLEDGMENTS

The authors acknowledge the National Science Foundation and the Sloan Foundation for partial support of this research.

- ¹M. C. Nuss, D. H. Auston, and F. Capasso, *Phys. Rev. Lett.* **58**, 2355 (1987).
- ²S. E. Ralph, Y. Chen, J. Woodall, and D. McInturff, *Phys. Rev. B* **54**, 5568 (1996).
- ³B. N. Flanders, D. C. Arnett, and N. F. Scherer, *IEEE J. Sel. Top. Quantum Electron.* **4**, 353 (1998).
- ⁴M. C. Beard, G. M. Turner, and C. A. Schmuttenmaer, *Phys. Rev. B* **62**, 15764 (2000).
- ⁵G. M. Turner, M. C. Beard, D. S. Venables, and C. A. Schmuttenmaer, in *Proceedings of the 10th Annual Symposium of the NSF Center Photoinduced Charge Transfer*, edited by L. Rothberg (World Scientific, New Jersey, 2000), p. 223.
- ⁶M. C. Beard, G. M. Turner, and C. A. Schmuttenmaer, in *Ultrafast Phenomena XII*, edited by T. Elsaesser, S. Mukamel, N. Scherer, and M. Murnane (Springer, Berlin, 2000).
- ⁷J. T. Kindt and C. A. Schmuttenmaer *J. Chem. Phys.* **110**, 8589 (1999).
- ⁸R. D. Averitt, G. Rodriguez, J. L. W. Siders, S. A. Trugman, and A. J. Taylor, *J. Opt. Soc. Am. B* **17**, 327 (2000).
- ⁹K. L. Shlager and J. B. Schneider, *IEEE Antennas Propag. Mag.* **37**, 39 (1995).
- ¹⁰K. S. Yee, *IEEE Trans. Antennas Propag.* **AP-14**, 302 (1966).
- ¹¹R. J. Luebbers, F. Hunsberger, and K. S. Kunz, *IEEE Trans. Antennas Propag.* **39**, 29 (1991).
- ¹²R. J. Luebbers and F. Hunsberger, *IEEE Trans. Antennas Propag.* **40**, 1297 (1992).
- ¹³P. G. Petropoulos, *IEEE Trans. Antennas Propag.* **42**, 62 (1994).
- ¹⁴W. H. Weedon and C. M. Rappaport, *IEEE Trans. Antennas Propag.* **45**, 401 (1997).
- ¹⁵R. M. Joseph, S. C. Hagness, and A. Taflove, *Opt. Lett.* **16**, 1412 (1991).
- ¹⁶N. Katzenellenbogen and D. Grischkowsky, *Appl. Phys. Lett.* **61**, 840 (1992).
- ¹⁷D. Grischkowsky, S. Keiding, M. Vanexter, and C. Fattinger, *J. Opt. Soc. Am. B* **7**, 2006 (1990).
- ¹⁸M. C. Beard, G. M. Turner, and C. A. Schmuttenmaer, *Phys. Rev. B* (submitted).
- ¹⁹D. F. Kelley and R. J. Luebbers, *IEEE Trans. Antennas Propag.* **44**, 792 (1996).
- ²⁰J. P. Berenger, *J. Comput. Phys.* **114**, 185 (1994).
- ²¹R. Holland and J. W. Williams, *IEEE Trans. Nucl. Sci.* **30**, 4583 (1983).
- ²²S. Mukamel, *Principles of Nonlinear Optical Spectroscopy* (Oxford University Press, New York, 1995).
- ²³D. Chandler, *Introduction to Modern Statistical Mechanics* (Oxford University Press, New York, 1987).
- ²⁴J. B. Marion, *Classical Dynamics of Particles and Systems*, 2nd ed. (Academic, New York, 1970).
- ²⁵L. D. Landau and E. M. Lifshitz, *Electrodynamics of Continuous Media*, 2nd ed. (Pergamon, New York, 1984).
- ²⁶J. T. Kindt and C. A. Schmuttenmaer, *J. Phys. Chem.* **100**, 10373 (1996).
- ²⁷W. H. Press, S. A. Teukolsky, W. T. Vetterling, and B. P. Flannery, *Numerical Recipes in Fortran*, 2nd ed. (Cambridge University Press, New York, 1986).
- ²⁸M. C. Beard, G. M. Turner, C. A. Schmuttenmaer, *J. Am. Chem. Soc.* **122**, 11541 (2000).